ChemComm

COMMUNICATION

View Article Online
View Journal | View Issue

Cite this: *Chem. Commun.*, 2019, **55**, 7065

Received 27th February 2019,
Accepted 1st May 2019

DOI: 10.1039/c9cc01675a

rsc.li/chemcomm

Nanofocused synchrotron X-ray absorption studies of the intracellular redox state of an organometallic complex in cancer cells†

Carlos Sanchez-Cano, ‡§*[a] Diego Gianolio,‡[b] Isolda Romero-Canelon, ¶[a] Remi Tucoulou[c] and Peter J. Sadler *[a]

Synchrotron nanoprobe X-ray absorption (XAS) studies of a potent organo-osmium arene anticancer complex in ovarian cancer cells at subcellular resolution allow detection and quantification of both Os^{II} and Os^{III} species, which are distributed heterogeneously in different areas of the cells.

The rich chemistry of transition metals allows them to undergo a wide variety of reactions inside cells.[1] Novel metallodrugs can be designed which reach diverse cellular targets and have unusual effects on biochemical pathways.[2] They offer a new strategy to help overcome tumour resistance to chemotherapy, a current clinical need.[3] However, elucidation of the effects of metallodrugs on biomolecular interactions in cells is a major challenge.[4]

The organometallic osmium half-sandwich, 'piano-stool' complex $[(\eta^6\text{-}p\text{-cym})Os(Azpy\text{-}NMe_2)I]^+$ (*p*-cym = *p*-cymene, Azpy-NMe_2 = 2-(*p*-((dimethylamino)phenylazo)pyridine)) **[1]** (Fig. 1a) is a promising anticancer drug candidate with interesting anticancer activity *in vitro* and *in vivo*.[5] The osmium complex penetrates readily into the core of tumours,[6] has a different mechanism of action from cisplatin and is capable of overcoming platinum resistance.[5] Complex **1** is a relatively inert prodrug that is activated by hydrolysis of the Os–I bond in a reducing environment inside cells,[7] and rapidly generates ROS efficiently through mitochondrial pathways.[8] *In vitro* experiments have shown that the reaction between **1** and GSH generates reactive analogues, including the hydroxido and chlorido complexes **1-OH** or **1-Cl**, respectively, which can bind to cysteine residues and generate $OH^{\bullet}$ radicals in the presence of hydrogen peroxide (Scheme S1, ESI†).[7] However, the nature of the derivatives of **1** involved in the cellular activity of the drug after intracellular activation is not understood. Here we use X-ray absorption spectroscopy (XAS) to investigate the chemical behaviour of **1** in cancer cells.

Synchrotron radiation is particularly suitable for exploring the chemical behaviour of metals in biological samples.[9] XAS is a powerful technique that can be used to obtain valuable information about the chemical state, and the electronic and structural properties of metals. This is achieved by using an X-ray beam of variable energy to probe the binding energy of electrons in specific electronic shells of the element (X-ray Absorption Near Edge Structure; XANES), or the elastic scattering processes between the photo-electrons generated by the incident beam and other atoms in the vicinity of the metal centre (Extended X-Ray Absorption Fine Structure, EXAFS) (Fig. S1, ESI†). The study of bulk cell populations (*e.g.* cell pellets or tissue samples)[10] and single cells (by using microprobe beamlines)[11] with these techniques has provided information on the oxidation state and speciation of several metallodrugs. Furthermore, state-of-the-art nanofocused synchrotron radiation allows imaging and spectroscopic techniques to be combined in studies of metal systems with subcellular resolution. However, although nano-XAS has allowed the chemical characterisation of nanomaterials with nanometre resolution,[12] sensitivity limits of the technique usually hamper its application for studies of metals inside cells.

To record meaningful XAS spectra using nanofocused synchrotron radiation, a metallodrug needs to be (1) present in high concentration inside cells (difficult to achieve when using biologically-relevant doses), or (2) concentrated within small specific areas of the cell. Recent X-ray fluorescence (XRF) maps of cells treated with **1** show a marked concentration of osmium within small organelles (probably mitochondria; supported by ICP-MS analysis of mitochondrial fractions extracted from the same cells).[13] Hence, we have investigated nano-XAS spectra of the Os L-edge in cells treated with **1** to provide new insight into its intracellular speciation.

[a] *Department of Chemistry, University of Warwick, Coventry, CV4 7AL, UK. E-mail: p.j.sadler@warwick.ac.uk*
[b] *Diamond Light Source, Harwell Science and Innovation Campus, Didcot, Oxon, OX11 0DE, UK*
[c] *ESRF, The European Synchrotron, 71 Avenue des Martyrs, 38000, Grenoble, France*

† Electronic supplementary information (ESI) available. See DOI: 10.1039/c9cc01675a

‡ These authors contributed equally to this work.

§ Current address: CIC biomaGUNE, Parque Científico y Tecnológico de Gipuzkoa, Paseo Miramón 182, 20014 San Sebastian, Spain. E-mail: csanchez@cicbiomagune.es

¶ Current address: School of Pharmacy, Institute of Clinical Sciences, University of Birmingham, Birmingham B15 2TT, UK.

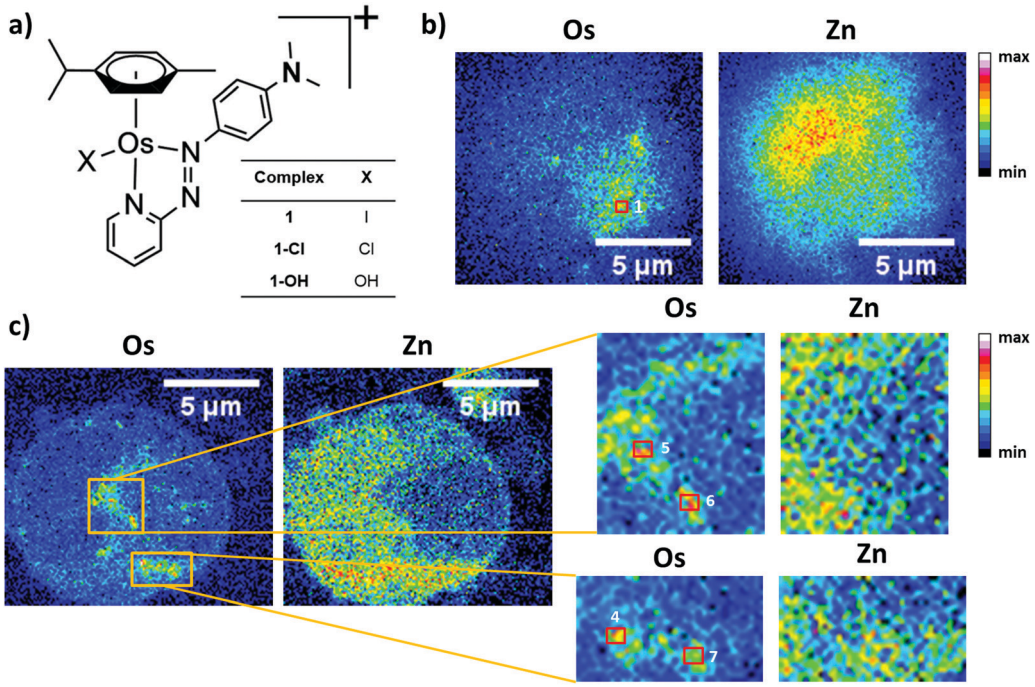

Fig. 1 (a) Structures of $[(\eta^6\text{-}p\text{-cym})Os(Azpy\text{-}NMe_2)I]^+$ **[1]** and substitution products. XRF maps showing the cellular distribution of Os and Zn in (b) cryo-fixed and dehydrated A2780 cells (CFD), and (c) 500 nm thick sections of A2780 cells (TS), treated for 24 h with 1 μM **1**. The red squares and white numbers indicate areas where nano-XAS spectra were recorded. Energy settings: 11.2 keV, flux 5×10^8 ph s^{-1}. Raster scan: 100×100 nm^2 step size, at 1 s dwell time.

We used hard X-rays (over 5–10 keV) focused on a 70×100 nm^2 spot size at the nano-analysis beamline ID16B[14] (ESRF) to record XAS spectra on selected areas of A2870 ovarian carcinoma cells treated for 24 h with 1 μM of **1**. Both 500 nm thick sections of epon embedded cells [TS] and whole cells cryo-fixed and then dehydrated [CFD] were studied.

This comparison was made to rule out the possibility that sample preparation for sections might affect the chemical form of **1** in cells. Initially, XRF maps were collected to detect areas with high concentrations of Os. As observed previously,[13] peaks corresponding to emissions resulting from excitation of the Os–L, Zn–K and Cu–K edges were observed for samples treated with **1** (Fig. S1 and S2, ESI†), independently of the sample fixation protocol used. XRF elemental maps confirmed that Os was highly concentrated in small areas within the cytoplasm of cells, and not in the nuclei, the latter regions being where high concentrations of Zn were found (Fig. 1 and Fig. S3, S4, ESI)†.

Nano-XAS Os L_3-edge spectra (probing $2p_{3/2}$ electrons; Fig. S1, ESI†) were recorded at ambient temperature for areas where XRF maps showed a high density of Os (red boxes in Fig. 1b, c and Fig. S3, S4, ESI†). The spectra displayed well-defined XANES and short EXAFS regions where some fine structures could be observed (Fig. 2a and Fig. S5, ESI†). The XAS spectra were recorded for a series of Os^{II} standards that might represent species that could be found inside cells, based on the *in vitro* activation experiments (**1**, **1-OH**, **1-Cl** and **1-SG**; Scheme S1 and Fig. S6, ESI†),[7] but also Os^0 to Os^{IV} standards to probe the oxidation state of intracellular Os species. Where possible, the S/N ratios were improved by averaging multiple scans obtained on each area (Table 1). Small drifts in the position of the beam were observed between individual acquisitions. This was compensated for by realigning the beam before each scan, but ultimately implied that the spatial resolution of the XAS measurements was slightly worse than the 70×100 nm^2 spot size. Data analysis is complicated for Os L-edges due to the large atomic size and atomic number of Os.[15] Remarkably, the ranges of energy of the incident X-rays used for obtaining the XAS spectra and wavenumber k ($Å^{-1}$) are related, and define the resolution for the measurement of interatomic distances between the metal and its coordination sphere. The longer these ranges are, the higher is the precision of the calculation on the length of these bonds. We were able to collect meaningful EXAFS only for wavenumbers up to $k = 8$ $Å^{-1}$ (Fig. S5c and d, ESI†), which proved to be too small to provide highly accurate information on the coordination sphere of the complex. Through XANES analysis it was also impossible to differentiate between **1** and its derivatives (*i.e.* **1-OH**, **1-Cl**, *etc.*; Fig. S6, ESI†), and therefore the speciation of **1** inside cells could not be fully determined.

Nonetheless, XANES spectra of Os standards with oxidation states between 0 and IV+ were significantly different (Fig. 2b and Fig. S7, ESI†). The small differences between the XANES of **1** and its analogues (Fig. S6, ESI†) suggest that changes observed for Os^0 to Os^{IV} standards should be mainly related to the oxidation state of the metal centers, and not to possible contributions from their coordination sphere. Interestingly, the spectra obtained from areas within cells appeared to be intermediate between Os^{II} and Os^{III} by comparison with standards (Fig. 2c and Fig. S8–S16, ESI†). Moreover, Linear Combination

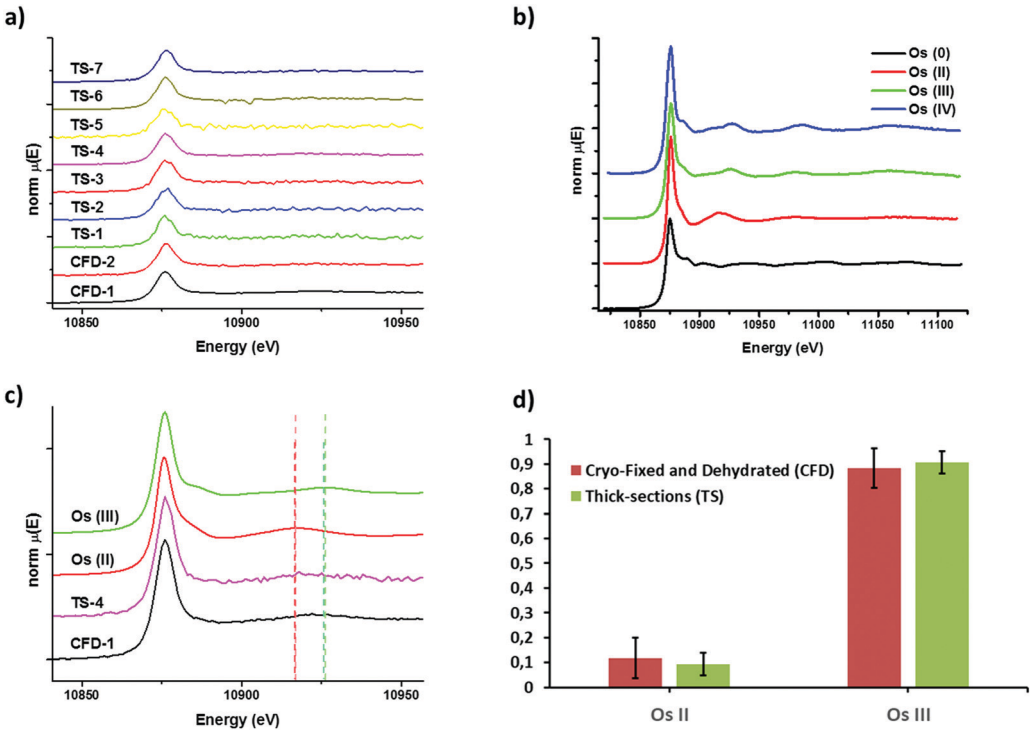

Fig. 2 (a) XANES spectra collected from areas with high densities of Os in cryo-fixed and dehydrated (CFD) or 500 nm thick sections (TS) of A2780 cells, treated for 24 h with 1 μM **1**; (b) XANES spectra of Os standards: Os powder (Os^0), **1** (Os^{II}), $OsCl_3$ (Os^{III}) and $[NH_4]_2OsCl_6$ (Os^{IV}) (c) XANES spectra of **1** (Os^{II}) and $OsCl_3$ (Os^{III}) standards, and spectra collected in positions CFD-1 and TS-5 (green and red dotted lines show maximum of secondary peaks for Os^{II} and Os^{III} standards); and (d) average ratio of Os^{II} and Os^{III} species found in CFD and TS samples. Scan: 10.82–11.12 keV; 1 eV step; 3 s accumulation; and 70 × 100 nm^2 beam size.

Table 1 Number of scans per sample and ratios of Os^{II} and Os^{III} species on areas of cryo-fixed and dehydrated (CFD) or 500 nm thick section (TS) cells, calculated as LCF from standards

Sample	Scans	Os^{II}	Os^{III}	Error	R-factor
CFD-1	40	0.04	0.96	0.05	0.0019
CFD-2	8	0.20	0.82	0.10	0.0041
TS-1	2	0.28	0.72	0.15	0.0117
TS-2	3	0.00	1.00	0.10	0.0099
TS-3	10	0.00	1.00	0.12	0.0122
TS-4	10	0.19	0.81	0.13	0.0261
TS-5	15	0.00	1.00	0.09	0.0467
TS-6	4	0.00	1.00	0.08	0.0061
TS-7	4	0.18	0.82	0.09	0.0075

Fitting (LCF, using the Os^{II} and Os^{III} standards) revealed high spatial heterogeneity, with different contributions of Os^{II} and Os^{III} oxidation states to the multiple spectra recorded (even when the areas studied were found within the same cell, Fig. 1, Table 1 and Fig. S4, ESI†). Between 0–30% Os^{II} and 100–70% Os^{III} species were found in the different areas analysed (Table 1). However, the overall ratio of Os^{II}/Os^{III} species found in each sample was constant and independent of the fixation method used (*ca.* 10% Os^{II} and 90% Os^{III}; Fig. 2d). Unfortunately, continuous irradiation of a solid sample of **1** for over 30 min using a microfocused beam with a similar flux density to the one used in our studies suggested that beam damage could cause some of the oxidation observed (Fig. S17, ESI†). The XRF elemental mapping involved irradiation of the samples for much shorter times (dwell time 1 s), avoiding unwanted oxidation. A higher number of scans improved the S/N ratios, but, in CFD samples, the irradiation time also appeared to correlate with observation of increasing quantities of Os^{III} in the areas studied (as calculated by LCF from standards; Table 1 and Fig. S18, ESI†). For sectioned cells (TS), in contrast, the relative quantities of Os^{II} and Os^{III} species were related to the spatial localisation of the cellular area studied, and not to the number of scans obtained (Fig. 3, Table 1 and Fig. S18, S19, ESI†). It was not possible to assess this on CFD samples since we analysed only one area per cell. Hence we cannot rule out the possibility that some beam damage might have occurred when multiple scans were obtained from individual areas of the cells (to improve the S/N ratio of XANES spectra). Nevertheless, this beam damage is not responsible for the differences observed in the speciation of Os, which is related to cellular localisation.

Overall, these studies show that meaningful nano-XAS spectra can be obtained from ovarian cancer cells treated with biologically-relevant concentrations of an Os-based candidate anticancer drug. Although no information on the coordination sphere of the complex could be obtained, a heterogeneous distribution of Os^{II} and Os^{III} species within the treated A2780 cells was observed. Such spatial variations in the speciation of the drug are interesting, and might be due to the presence of: (1) different degrees of oxidation of **1** within the areas studied, or (2) an intracellular redox cycle as part of the mechanism of

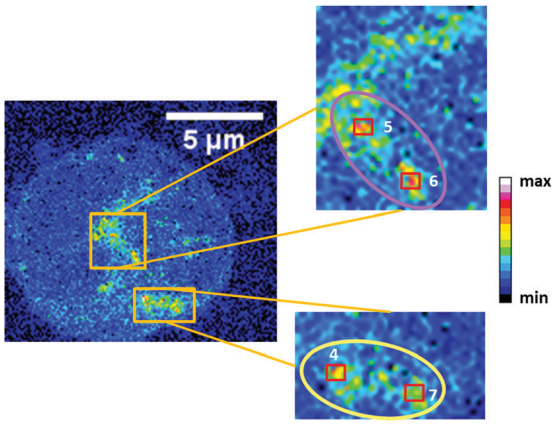

Fig. 3 XRF maps of 500 nm thick sections of A2780 cells treated for 24 h with 1 μM **1** showing cellular distribution of Os. The red squares and white numbers indicate areas where nano-XAS spectra were recorded. The ellipses indicate areas with 100% Os^{III} (purple) or 20% Os^{II} and 80% Os^{III} species (yellow).

action of the drug. Remarkably, biometals such as Fe and Cu can generate $OH^{\bullet}$ radicals inside cells in the presence of H_2O_2 through redox-dependent reactions.[16] A similar redox cycle involving Os^{II}/Os^{III} species could explain the ROS increase observed when cells are treated with **1**. However, additional experiments are needed to fully understand the mechanism responsible for the intracellular generation of Os^{III} species, and its importance in the anticancer mechanism of action of **1**.

XRF and XAS were obtained in the frame of the ESRF proposal CH-4714. We thank Dr Tina Geraki (I18, Diamond light source) for help with beam damage measurements, the CRUK/EPSRC (Grant No. C53561/A19933), the EPSRC (Grant No. EP/F034210/1) and the Wellcome Trust (Grant No. 107691/Z/15/Z) for financial support.

Conflicts of interest

There are no conflicts to declare.

References

1 K. L. Haas and K. J. Franz, *Chem. Rev.*, 2009, **109**, 4921; E. A. Hillard and G. Jaouen, *Organometallics*, 2011, **30**, 20; D. Rehder and E. Nordlander, *Bioinorganic Chemistry: An Introduction*, 2014; Y. Bai, J. Chen and S. C. Zimmerman, *Chem. Soc. Rev.*, 2018, **47**, 1811.
2 U. Jungwirth, C. R. Kowol, B. K. Keppler, C. G. Hartinger, W. Berger and P. Heffeter, *Antioxid. Redox Signaling*, 2011, **15**, 1085; A. de Almeida, B. L. Oliveira, J. D. G. Correia, G. Soveral and A. Casini, *Coord. Chem. Rev.*, 2013, **257**, 2869; K. D. Mjos and C. Orvig, *Chem. Rev.*, 2014, **114**, 4540; J. J. Soldevila-Barreda and P. J. Sadler, *Curr. Opin. Chem. Biol.*, 2015, **25**, 172; C. S. Allardyce and P. J. Dyson, *Dalton Trans.*, 2016, **45**, 3201; Z. Yu and J. A. Cowan, *Chem. – Eur. J.*, 2017, **23**, 14113.
3 A. I. Minchinton and I. F. Tannock, *Nat. Rev. Cancer*, 2006, **6**, 583; L. Kelland, *Nat. Rev. Cancer*, 2007, **7**, 573.
4 C. A. Wotton, C. Sanchez-Cano, H. K. Liu, M. P. Barrow, P. J. Sadler and P. B. O'Connor, *Dalton Trans.*, 2015, **44**, 3624; R. F. S. Lee, L. Menin, L. Patiny, D. Ortiz and P. J. Dyson, *Anal. Chem.*, 2017, **89**, 11985; C. A. Wootton, C. Sanchez-Cano, A. F. Lopez-Clavijo, E. Shaili, M. P. Barrow, P. J. Sadler and P. B. O'Connor, *Chem. Sci.*, 2018, **9**, 2733.
5 Y. Fu, A. Habtemariam, A. M. Pizarro, S. H. van Rijt, D. J. Healey, P. A. Cooper, S. D. Shnyder, G. J. Clarkson and P. J. Sadler, *J. Med. Chem.*, 2010, **53**, 819; S. D. Shnyder, Y. Fu, A. Habtemariam, S. H. Van Rijt, P. A. Cooper, P. M. Loadman and P. J. Sadler, *Med. Chem. Commun.*, 2011, **2**, 666.
6 C. Sanchez-Cano, I. Romero-Canelón, K. Geraki and P. J. Sadler, *J. Inorg. Biochem.*, 2018, **185**, 26.
7 R. J. Needham, C. Sanchez-Cano, X. Zhang, I. Romero-Canelón, A. Habtemariam, M. S. Cooper, L. Meszaros, G. J. Clarkson, P. J. Blower and P. J. Sadler, *Angew. Chem., Int. Ed.*, 2017, **56**, 1017.
8 J. M. Hearn, I. Romero-Canelon, A. F. Munro, Y. Fu, A. M. Pizarro, M. J. Garnett, U. McDermott, N. O. Carragher and P. J. Sadler, *Proc. Natl. Acad. Sci. U. S. A.*, 2015, **112**, E3800; I. Romero-Canelon, M. Mos and P. J. Sadler, *J. Med. Chem.*, 2015, **58**, 7874.
9 B. Gilbert, S. C. Fakra, T. Xia, S. Pokhrel, L. Madler and A. E. Nel, *ACS Nano*, 2012, **6**, 4921; L. Wang, T. Zhang, P. Li, W. Huang, J. Tang, P. Wang, J. Liu, Q. Yuan, R. Bai, B. Li, K. Zhang, Y. Zhao and C. Chen, *ACS Nano*, 2015, **9**, 6532; G. Veronesi, C. Aude-Garcia, I. Kieffer, T. Gallon, P. Delangle, N. Herlin-Boime, T. Rabilloud and M. Carriere, *Nanoscale*, 2015, **7**, 7323.
10 M. D. Hall, G. J. Foran, M. Zhang, P. J. Beale and T. W. Hambley, *J. Am. Chem. Soc.*, 2003, **125**, 7524; M. D. Hall, C. T. Dillon, M. Zhang, P. Beale, Z. Cai, B. Lai, A. P. J. Stampfl and T. W. Hambley, *J. Biol. Inorg. Chem.*, 2003, **8**, 726; P. D. Bonnitcha, M. D. Hall, C. K. Underwood, G. J. Foran, M. Zhang, P. J. Beale and T. W. Hambley, *J. Inorg. Biochem.*, 2006, **100**, 963; K. L. Munro, A. Mariana, A. I. Klavins, A. J. Foster, B. Lai, S. Vogt, Z. Cai, H. H. Harris and C. T. Dillon, *Chem. Res. Toxicol.*, 2008, **21**, 1760; J. B. Aitken, A. Levina and P. A. Lay, *Curr. Top. Med. Chem.*, 2011, **11**, 553; M. D. Hall, H. L. Daly, J. Z. Zhang, M. Zhang, R. A. Alderden, D. Pursche, G. J. Foran and T. W. Hambley, *Metallomics*, 2012, **4**, 568; A. A. Hummer, P. Heffeter, W. Berger, M. Filipits, D. Batchelor, G. E. Buchel, M. A. Jakupec, B. K. Keppler and A. Rompel, *J. Med. Chem.*, 2013, **56**, 1182; A. K. Renfrew, N. S. Bryce and T. W. Hambley, *Chem. Sci.*, 2013, **4**, 3731; C. K. J. Chen, J. Z. Zhang, J. B. Aitken and T. W. Hambley, *J. Med. Chem.*, 2013, **56**, 8757.
11 F. Reith, B. Etschmann, C. Grosse, H. Moors, M. A. Benotmane, P. Monsieurs, G. Grass, C. Doonan, S. Vogt, B. Lai, G. Martinez-Criado, G. N. George, D. H. Nies, M. Mergeay, A. Pring, G. Southam and J. Brugger, *Proc. Natl. Acad. Sci. U. S. A.*, 2009, **106**, 17757; A. D. Servin, H. Castillo-Michel, J. A. Hernandez-Viezcas, B. Corral Diaz, J. R. Peralta-Videa and J. L. Gardea-Torresdey, *Environ. Sci. Technol.*, 2012, **46**, 7637; B. Etschmann, J. Brugger, L. Fairbrother, C. Grosse, D. H. Nies, G. Martinez-Criado and F. Reith, *Chem. Geol.*, 2016, **438**, 103; L. E. Wu, A. Levina, H. H. Harris, Z. Cai, B. Lai, S. Vogt, D. E. James and P. A. Lay, *Angew. Chem., Int. Ed.*, 2016, **55**, 1742.
12 J. Segura-Ruiz, G. Martínez-Criado, M. H. Chu, S. Geburt and C. Ronning, *Nano Lett.*, 2011, **11**, 5322; J. Segura-Ruiz, G. Martınez-Criado, M. H. Chu, C. Denker, J. Malindretos and A. Rizzi, *J. Appl. Phys.*, 2013, **113**, 136511; A. Kuzmina and J. Chaboy, *IUCrJ*, 2014, **1**, 571; G. Martínez-Criado, J. Segura-Ruiz, B. Alen, J. Eymery, A. Rogalev, R. Tucoulou and A. Homs, *Adv. Mater.*, 2014, **26**, 7873; G. Marínez-Criado, J. Segura-Ruiz, M. H. Chu, R. Tucoulou, I. López, E. Nogales, B. Mendez and J. Piqueras, *Nano Lett.*, 2014, **14**, 5479; J. Segura-Ruiz, G. Martínez-Criado, C. Denker, J. Malindretos and A. Rizzi, *Nano Lett.*, 2014, **14**, 1300.
13 C. Sanchez-Cano, I. Romero-Canelon, Y. Yang, I. Hands-Portman, S. Bohic, P. Cloetens and P. J. Sadler, *Chem. – Eur. J.*, 2017, **23**, 2512.
14 G. Martínez-Criado, J. Villanova, R. Tucoulou, D. Salomon, J. P. Suuronen, S. Labouré, C. Guilloud, V. Valls, R. Barrett, E. Gagliardini, Y. Dabin, R. Baker, S. Bohic, C. Cohen and J. Morsea, *J. Synchrotron Radiat.*, 2016, **23**, 344.
15 K. A. Lomachenko, C. Garino, E. Gallo, D. Gianolio, R. Gobetto, P. Glatzel, N. Smolentsev, G. Smolentsev, A. V. Soldatov, C. Lamberti and L. Salassa, *Phys. Chem. Chem. Phys.*, 2013, **15**, 16152; A. Pitto-Barry, K. Geraki, M. D. Horbury, V. G. Stavros, J. F. W. Mosselmans, R. I. Walton, P. J. Sadler and N. P. E. Barry, *Chem. Commun.*, 2017, **53**, 12898.
16 M. Valko, K. Jomova, C. J. Rhodes, K. Kuca and K. Musilek, *Arch. Toxicol.*, 2016, **90**, 1.